Photoelectron emission microscopy of ultrathin oxide covered devices

V. W. Ballarotto[a)]
The Laboratory for Physical Sciences, 8050 Greenmead Drive, College Park, Maryland 20740

M. Breban, K. Siegrist, R. J. Phaneuf, and E. D. Williams
Department of Physics, University of Maryland, College Park, Maryland 20742

(Received 30 May 2002; accepted 7 October 2002)

Photoelectron emission microscopy (PEEM) has been used to investigate simple device structures buried under ultrathin oxides. In particular, we have imaged Au–SiO_2 and *p*-type Si–SiO_2 structures and have demonstrated that PEEM is sensitive to these buried structures. Oxide overlayers ranging up to 15.3 nm were grown by systematically varying the exposure time of the structures to a plasma-enhanced chemical-vapor deposition process. The change in image contrast as the oxide thickness increases was used to quantify the inelastic mean-free path of low-energy photoelectrons (~1 eV) in amorphous silicon dioxide. For Au structures we find that the dominant mean-free path for photoelectrons in the overlying oxide is about 1.18 ± 0.2 nm. Yet, we find a residual observable signal from the buried Au structure through roughly 13 oxide attenuation lengths. The signal attenuation from the Au can be explained by the spread of the photoelectron energies and the energy dependence of the electron–phonon interaction. Similar intensity attenuation behavior is also seen from heavily *p*-doped silicon (10^{20} cm^{-3}) regions, but the signal is only observable through roughly 3.0 nm of oxide, and the signal from the 10^{18} cm^{-3} regions is not detectable through the thinnest oxide layer of approximately 2.5 nm. Here, the energy spread (~2.0 eV) is more narrowly distributed about the phonon loss energies, leading to the observed attenuation behavior from heavily *p*-doped silicon. © *2002 American Vacuum Society.* [DOI: 10.1116/1.1525007]

I. INTRODUCTION

Photoelectron emission microscopy (PEEM) has matured to the point where it can be used for practical applications. To evaluate potential applications in semiconductor device metrology, we have been using PEEM to image simple model devices so that basic contrast mechanisms can be characterized and used in analysis of integrated circuits. Analysis of integrated circuits with PEEM requires knowledge of the implant regions, metal layers, and the intervening dielectric. To accomplish this, we have previously studied and modeled contrast due to doping.[1–3] Here, we present the extension of this work to image analysis of buried metal and implanted structures.

The ability to detect either buried implant patterns or metal lines without removing the overlying oxide layer would allow rapid, nondestructive imaging of buried device structures. Continual miniaturization of Si-based technology has led to the use of ultrathin oxides, thus imaging structures buried under nanometer-thick oxide layers has become more relevant. Several microscopic techniques such as plan-view transmission electron microscopy[4,5] and scanning reflection electron microscopy[6,7] have been used to examine the buried SiO_2/Si interface. There have also been several PEEM studies on buried interfaces.[8,9] However, we are unaware of any imaging studies that have been done on oxide-covered Au lines or implant structures.

We present a study in which PEEM is used to investigate simple device structures buried under ultrathin oxides. Specifically, Au lines and *p*-type Si implant patterns covered with ultrathin oxides of various thicknesses are imaged. Since we are imaging photoelectrons that were emitted near threshold, transport through the overlying oxide and image formation is accomplished with extremely low-energy photoelectrons. This leads to some surprising behavior in evolution of contrast with oxide thickness.

II. EXPERIMENT

Several test structures with variable oxide thicknesses over a pattern of Au lines and boron implants in silicon were fabricated. Photolithography was used to produce structures with feature sizes that vary from 2 to 10 μm. Gold was chosen because it is typically used for electron attenuation measurements. The gold structures, approximately 50 nm thick on a native oxide-covered lightly doped *n*-type Si(100) substrate, were produced by thermal evaporation through a mask. After deposition of the metal films, the samples were cleaned with a low-power (100 W) oxygen plasma. The patterned *p*-type regions were formed by broad beam implantation of boron (10^{18} and 10^{20} cm^{-3}, 190 keV) through a mask into a lightly doped *n*-type Si substrate. Both sets of samples are then exposed to a plasma-enhanced chemical-vapor deposition (PECVD) process for increasing times to systematically increase the thickness of the silicon dioxide overlayer. Sample replicates were subsequently etched with an etch mask in place to produce trenches so that profilometry could be used to measure the film thickness in 5–6 different places. The average deposition rate of the amorphous film when the substrate is at 300 °C is 15 ± 2.2 nm/min. The av-

a)Electronic mail: vince@lps.umd.edu

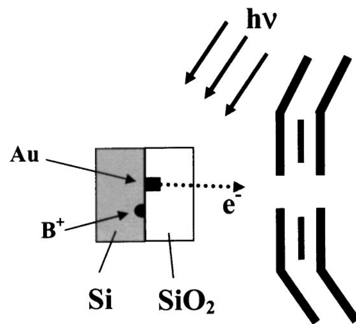

FIG. 1. Schematic of the experimental setup. The objective lens of the PEEM and a generic sample are depicted. In the actual experiment, SiO_2 of various thicknesses covers either Au lines or B-implanted patterns on a lightly *n*-doped Si substrate.

erage index of refraction of the resulting oxide films is 1.484. We refer to samples that only the native oxide covers the surface as null samples.

The PEEM setup has been described in previous work.[3] For this application we will also briefly describe the imaging situation at the buried interface. Light from a Hg short-arc lamp ($h\nu_{max}$~5.15 eV) passes through the oxide layer and is absorbed by either the underlying implanted silicon regions or the Au structures or the Si substrate, as illustrated in Fig. 1. For light of sufficient energy (~5.15 eV for Si or ~3.8 eV for Au), a distribution of photoelectrons will be excited into the conduction band of the oxide, and if the photoelectron energy is greater than the surface barrier at the oxide–vacuum interface, the electron will be emitted into the vacuum (see Fig. 2).

After fabrication, all the samples were mounted on a 3 in. wafer, which allows the individual samples to be moved sequentially into imaging position. Thus, the devices can be imaged with the same imaging conditions, allowing intersample comparison of image intensities. Once the imaging conditions for the weakest intensity sample were determined, the remaining samples were then imaged with the same conditions. Since the dynamic range of the detector is smaller than the change in intensity from the null sample to the thinnest oxide overlayer sample, a calibration curve of the null sample intensity was constructed. The intensity from the null sample was measured as the camera exposure time was decreased (typically, 3–4 steps) from a time interval where the image intensity just saturated the detector to a time interval where the image intensity level was comparable to that from the thinnest oxide overlayer sample. The intensity level from the null sample was then extrapolated for the exposure time used to measure the attenuation curve. Quantitative assessment of the resulting PEEM image intensity is done by averaging 200–300 sets of parallel line scans from the image data obtained from a 12 bit charge-coupled-device camera. The 12 bit images are stored in 16 bit files for image analysis.

III. RESULTS

As expected, we observe a strong PEEM signal from the Au lines when no deposited oxide overlayer covers the device (null sample). In Fig. 3(a), we show an image of the device with 2.5 nm of oxide overlayer. The Au lines are the brighter regions. The signal intensity from the 2.5 nm oxide-covered Au structures is reduced on average about 50 times compared to the null sample. For comparison, an image of a device with an oxide overlayer of 3.9 nm at the same detector gain is shown in Fig. 3(b). Both images in Fig. 3 have been averaged eight times. We show in Fig. 4 a plot of the

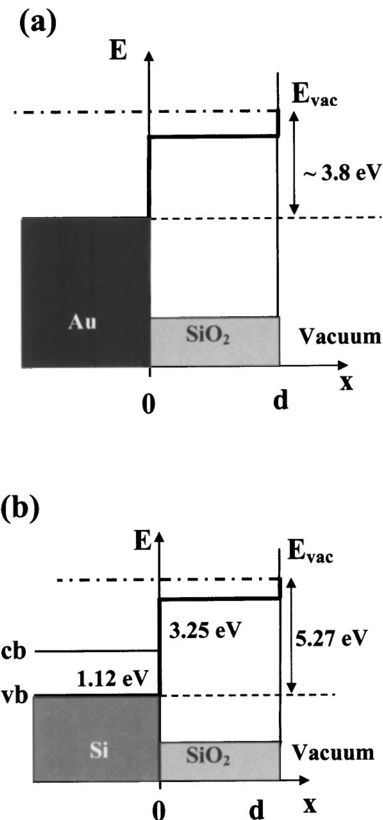

FIG. 2. Band diagrams of the different sample interfaces. (a) For the Au/SiO_2 interface, the photothreshold for an electron in Au to be excited into the vacuum is approximately 3.8 eV. (b) Photothreshold (~5.27 eV) for an electron in the Si valence band to be excited into vacuum is equal to the sum of the Si band gap (1.12 eV), conduction-band offset for SiO_2/Si interface (~3.25 eV), and the electron affinity of SiO_2 (0.9 eV). The maximum photon energy from the Hg lamp is approximately 5.15 eV. Without considering impurity band-tailing effects, photoelectrons from the Si valence band are ~0.1 eV short of being able to escape into vacuum.

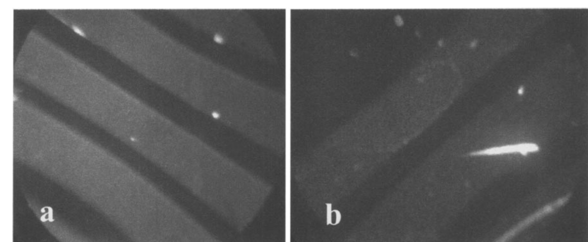

FIG. 3. PEEM images of a Au sample with two different oxide thicknesses. The brighter stripes are the Au lines: (a) 2.5 nm of oxide overlayer and (b) 3.9 nm of oxide overlayer. Bright features in the images are due to adventitious particles. The images have been averaged eight times and the field of view for both is 75 μm.

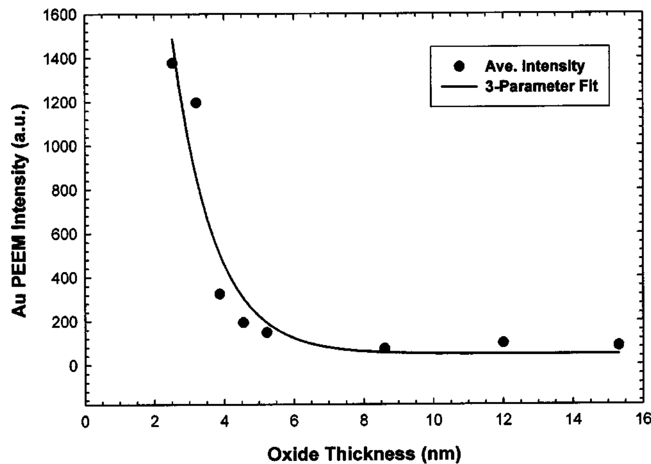

FIG. 4. Attenuation of the PEEM signal from Au as a function of CVD oxide thickness. The attenuation length is 1.18±2.0 nm. Note the persistent low-level signal for the thicker oxides.

average PEEM intensity from the Au lines as a function of the overlying oxide thickness. The data points in the graph represent the difference between the Au intensity and the intensity from the Si substrate (lightly n doped). The data are fitted with a three-parameter exponential decay model: $I = I_b + I_0 \exp(-z/\lambda)$, where z is the thickness of the oxide layer and λ is the signal attenuation length. We find the average signal attenuation length λ, or equivalently the electron inelastic mean-free path, is 1.18 ± 0.2 nm. To properly fit the low-intensity tail in the data, a constant background intensity term I_b must be included. Unexpectedly, a weak but discernible signal corresponding to the device pattern is still observable through approximately 15 nm of oxide. This corresponds to signal detection through roughly 13λ of the oxide.

Similar intensity attenuation behavior is also seen from heavily p-doped silicon. In Fig. 5(a), we show a wide field of view (~300 μm) image of a boron-implanted sample with no oxide. This image was not corrected for distortion. The line triplet in the center of the image (denoted by the top arrow) consists of a bright 3-μm-wide line with a boron concentration of 10^{20} cm^{-3} and a pair of 2-μm-wide lines, one to each side, with a boron concentration of 10^{18} cm^{-3}. The small dots are adventitious particles. Figure 5(b) illustrates that the signal from the 10^{20} cm^{-3} line is detectable as the oxide layer is increased to approximately 2.5 nm. The inten-

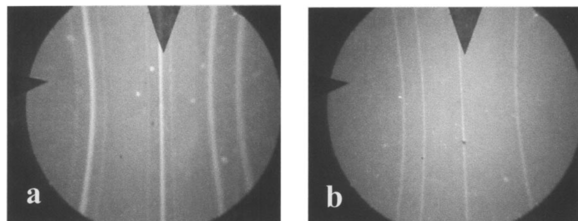

FIG. 5. PEEM images of the B-implanted sample with two different oxide thicknesses: (a) null sample and (b) 2.5 nm of oxide. The sample in image in (b) is rotated 180° relative to (a). Both images have been averaged 64 times and the field of view for both is about 300 μm. Images have not been corrected for distortion.

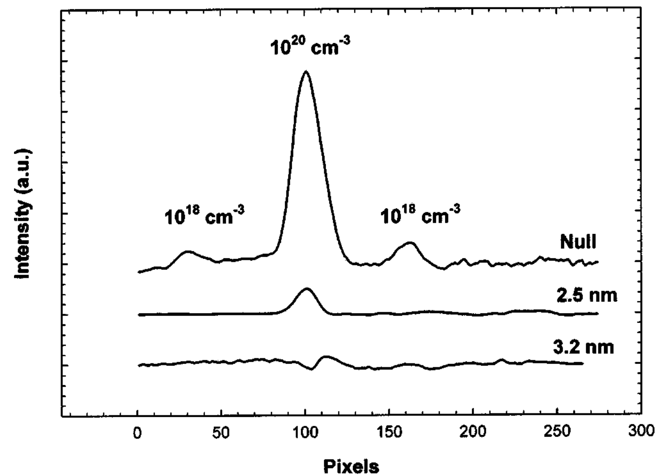

FIG. 6. Line scans across the triplet of lines denoted by the top arrow in Fig. 5. In the null sample, all three lines are observable (top trace). However, the 10^{18} cm^{-3} line pair is no longer observable at 2.5 nm of oxide (middle trace). At 3.2 nm of oxide, the dip at approximately pixel 105 indicates contrast reversal between 10^{20} cm^{-3} and the lightly n-doped substrate (bottom trace).

sity from the 10^{20} cm^{-3} line has decreased by roughly 85% as compared to the intensity from the null sample, and the apparent linewidth has decreased by a factor of 2/3. However, the 10^{18} cm^{-3} line pair is no longer observable at this oxide thickness. Interestingly, we find that as the oxide thickness is increased to about 3.2 nm, the intensity from the 10^{20} cm^{-3} line has decreased to below the background signal intensity from the n-type substrate. This reversal in contrast is observed up to an oxide thickness of 4.5 nm. For thicker oxide overlayers, the image signal decreases below detectable limits. In Fig. 6, we show a series of line scans across the implanted regions near the top arrow that illustrates the change in image intensity from the 10^{20} cm^{-3} regions as the oxide becomes thicker. The signal attenuation is too rapid to do a meaningful fit to the data in this case.

IV. DISCUSSION

We have been able to image Au structures buried under ultrathin layers of oxide (2.5–15 nm) with PEEM. The decrease in the signal intensity from the Au lines as the oxide overlayer increases is expected. The measured Au signal attenuation length of 1.18 nm also seems reasonable based upon an extrapolation of the measurements of Himpsel *et al.*[10] While there may be some question in equating the measured attenuation length to the inelastic mean-free path, Powell and Jablonski have shown in x-ray photoelectron spectroscopy measurements that the effective attenuation length for electrons in SiO_2 is approximately 90% of the inelastic mean-free path.[11] The persistent low-level image intensity as the oxide thickness increases beyond 6 nm has revealed that PEEM is unexpectedly sensitive to buried structures. If the measured image intensity were to simply fall off exponentially, then the signal from a Au structure covered with 6 nm of oxide would be about a thousand times smaller than the initial signal intensity. Instead, the low-level

intensity from the Au structures in the thicker oxide samples is about 9% of the intensity measured through one attenuation length (2.5 nm) of oxide. The barrier for photoemission for the oxide-covered Au structure is about 3.8 eV.[12] Therefore, a photoelectron has sufficient energy ($\sim$1.35 eV, in excess) to overcome the barrier to emission with our light source. This suggests that the low-level image intensity is probably due to a distribution of low-energy photoelectrons that still has sufficient energy to overcome the barrier at the oxide–vacuum interface after undergoing a number of inelastic collisions in the oxide.

When electrons are moving through the conduction band of the oxide overlayer with energy less than $2E_{\mathrm{gap}}$, there is a probability that they will interact with the lattice vibrations of SiO_2.[13] When this interaction leads to the creation of a phonon, an electron will lose energy ΔE_{vib}. For sufficient energy loss, the electron mobility can be reduced considerably and lead to charge trapping.[13] Both experimental and theoretical studies have shown that there is a pair of broad vibrational modes associated with the asymmetric stretching vibration of the bridging oxygen in a network of SiO_2 tetrahedra.[14,15] This asymmetric motion gives rise to a transverse optical (TO) phonon at 1065 cm^{-1} and a longitudinal optical (LO) phonon at 1252 cm^{-1}. There are also vibrational modes at lower wave numbers (634 and 670 cm^{-1}) that must be taken into account. Thus, the low-energy photoelectrons that are generated by internal photoemission in our samples have energy loss channels available at about 80 meV (the low-energy phonons), 130 meV (TO mode), and 150 meV (LO mode). The probability of an electron scattering with a phonon increases as the electron energy decreases,[13] dropping abruptly to zero, of course, once the threshold excitation energy is crossed. For example, the probability of a 1.35 eV photoelectron scattering inelastically with a LO phonon is 1.5 times more likely than scattering with the vibrational mode at 670 cm^{-1}. At an energy of 0.2 eV, the probability of an electron interacting with either the low-energy phonons or the optical phonons is equally likely. For energies less than 0.2 eV, energy loss is increasingly dominated by creation of low-energy phonons.

Initially, the majority of photoelectrons (those with $E > 0.2$ eV) lose their excess energy by interacting with the LO and TO modes of the oxide. A smaller fraction of the electrons (those with $E < 0.2$ eV) will lose energy primarily to the phonons at 634 and 670 cm^{-1}. As the distribution of electrons propagates through the oxide and loses energy, the energy loss mechanism gradually changes from being dominated by inelastic scattering with optical phonons to being dominated by low-energy phonon scattering (80 meV).

The attenuation curve for the buried Au structures can now be explained in terms of the energy distribution (0–1.35 eV) of the photoelectrons emitted from the Au. The high-energy electrons ($\sim$1.35 eV) will undergo approximately eight inelastic scattering events, due to optical phonon creation, before low-energy phonon scattering becomes the important energy loss mechanism. An additional three inelastic scattering events must occur before the electron energies decrease below the surface barrier. Thus, the low-intensity tail of the attenuation curve is due to the fraction of high-energy electrons ($\sim$1.35 eV) that have escaped over the surface barrier before undergoing approximately 11 scattering events. The observed signal cutoff occurs at an oxide thickness of approximately 15 nm, which is within the experimental uncertainty of 11 times the average measured attenuation length of 1.18 nm.

For buried implant structures, the attenuation behavior is more complex than for Au. Only photoelectrons from the *p*-type 10^{20} cm^{-3} lines can be detected for the thinnest PECVD oxide investigated. By analogy to the observation for the Au lines, one might expect that stripes of both doping levels should be observable but that the intensity would be less than that from the null sample. For simplicity, we assume that the density of interface states is sufficiently low ($<10^{12}$ cm^{-2}) so that no Fermi level pinning occurs, and as a result no band bending occurs. The flatband photothreshold ($\sim$5.27 eV) is the sum of the Si band gap (1.12 eV), the SiO_2/Si conduction-band offset [3.25 eV (Refs. 16–19)] and the electron affinity of SiO_2 [0.9 eV (Ref. 20)]. Thus, the photoelectrons from the Si valence band would be approximately 0.1 eV below the vacuum level when imaging with a Hg lamp [see Fig. 2(b)]. However, we know from our previous work that the photothreshold for 10^{20} cm^{-3} is less than the photothreshold for 10^{18} cm^{-3}.[2] One reason for this reduction in the photothreshold is that band tailing in heavily doped Si reduces the band gap.[21] Wagner has shown for boron doping concentrations between 10^{18} and 10^{20} cm^{-3}, the band gap is reduced by 50–200 meV.[22] Therefore, in our boron-implanted devices only the photothreshold for the 10^{20} cm^{-3} lines is sufficiently reduced to allow photoelectrons to be imaged through the oxide. The maximum energy of the distribution of photoelectrons from the valence band of 10^{20} cm^{-3} lines is approximately 0.2 eV. At this energy, all the energy loss channels due to phonon creation are equally likely. In addition, only three inelastic scattering events with phonons are necessary for the electron energies to decrease below the vacuum level. Hence, the signal from the 10^{20} cm^{-3} regions attenuates very quickly.

Contrast reversal observed in the thicker oxide B-implanted samples could be due to a contribution from the interface states to photoemission. The distribution of electrons from the interface states will have more energy than those from the valence band. Since the Fermi level for the *n* region is closer to the vacuum level, the maximum energy of electrons from this region will be slightly higher than for electrons from the 10^{20} cm^{-3} lines. Thus, the electrons from the *n* region will need to create more phonons and as a consequence travel further before they lose enough energy to fall below the surface barrier. Therefore, the signal from the 10^{20} cm^{-3} lines will attenuate faster than the signal from the substrate, resulting in contrast reversal.

Since the light source used for imaging has a continuous spectrum with several intensity peaks in the visible regime, we cannot rule out the possibility of photoemission from shallow defect states in the oxide layer. It is reasonable to

assume that the defects are located homogeneously throughout the oxide. Consequently, photoemission from the defects in the oxide would generate a uniform PEEM image intensity from the oxide. Image analysis subtracts a uniform background, and thus the effect makes little contribution to the observed contrast.

We note that it would be interesting to image our oxide-covered devices with a tunable energy photon source.[2] Varying the photon energy would generate photoelectrons with different energy distributions, which would permit investigation of the energy loss details in the oxide. Tuning the light source to a low energy would also determine if a second-order effect, such as photoemission from an electron trap state that has captured a photoelectron previously emitted from the underlying structure, contributes to the total image current density. In addition, imaging a new device with a wide range of boron concentrations would give a more precise determination of the photoyield cutoff. It is also necessary to test our assumption of flatbands by measuring the density of interface states with an independent technique like electron spin resonance.

Finally, we want to emphasize that the distribution of electrons transported through the oxide does not consist of hot carriers. The energy gain from the applied field strength in the oxide (10^6 V/m) is on the order of 50 meV. This field strength is well below the typical field strengths (10^8 V/m) used for charge injection into insulators.[23] Hence, electron transport through the oxide, and thus PEEM image formation, is occurring in a unique regime.

V. CONCLUSIONS

We have observed PEEM's surprising sensitivity to buried structures. Low-level signals from both Au and *p*-type Si structures have been observed when covered with ultrathin oxides. By quantifying the change in PEEM contrast as a function of overlying oxide thickness, we have been able to measure an electron mean-free path in SiO_2 of 1.18 nm. Attenuation of the Au signal can be explained quite reasonably by considering inelastic scattering of the photoelectrons with optical and low-energy phonons in the oxide. The signal from heavily *p*-doped Si is attenuated very quickly by the phonons in the oxide because of the near match in energy between the excited photoelectron and the vibrational modes of the oxide. Photothreshold reduction due to impurity band-tailing effects means that only the 10^{20} cm^{-3} regions and not the 10^{18} cm^{-3} lines could be imaged. In addition, the contrast reversal in the boron-implanted devices may be explained by the fact that more electron–phonon scattering events are necessary for electrons from the lightly *n*-doped substrate region than from the 10^{20} cm^{-3} before falling below the surface barrier. Therefore, the 10^{20} cm^{-3} regions will appear darker than the substrate for oxides thicker than about 3.0 nm.

ACKNOWLEDGMENTS

The authors would like to thank William Vanderlinde and also acknowledge the technical support provided by the Device Processing Staff at the Laboratory for Physical Sciences. This work was partially supported by the NSF-MRSEC.

[1]V. W. Ballarotto, K. Siegrist, R. J. Phaneuf, and E. D. Williams, J. Appl. Phys. **91**, 469 (2002).
[2]V. W. Ballarotto, K. Siegrist, R. J. Phaneuf, E. D. Williams, W.-C. Yang, and R. J. Nemanich, Appl. Phys. Lett. **78**, 3547 (2001).
[3]V. W. Ballarotto, K. Siegrist, R. J. Phaneuf, E. D. Williams, and S. Mogren, Surf. Sci. **461**, L570 (2000).
[4]J. M. Gibson and M. Y. Lanzerotti, Nature (London) **340**, 128 (1989).
[5]F. M. Ross and J. M. Gibson, Phys. Rev. Lett. **68**, 1782 (1992).
[6]H. Watanabe, K. Fujita, and M. Ichikawa, Surf. Sci. **385**, L952 (1997).
[7]W. Watanabe, K. Kato, T. Uda, K. Fujita, M. Ichikawa, Y. Kawamura, and K. Terakura, Phys. Rev. Lett. **80**, 345 (1998).
[8]H. Ade, W. Yang, S. L. English, J. Hartman, R. F. Davis, R. J. Nemanich, V. N. Litvinenko, I. V. Pinayev, Y. Wu, and J. M. J. Madey, Surf. Rev. Lett. **5**, 1257 (1998).
[9]J. Almeida, C. Coluzza, T. dell Orta, F. Barbo, M. Bertolo, A. Bianco, S. Cerasari, S. Fontana, and G. Margaritondo, J. Appl. Phys. **80**, 1460 (1996).
[10]F. J. Himpsel, F. R. McFeely, A. Taleb-Ibrahimi, J. A. Yarmoff, and G. Hollinger, Phys. Rev. B **38**, 6084 (1988).
[11]C. J. Powell and A. Jablonski, J. Electron Spectrosc. Relat. Phenom. **114-116**, 1139 (2001).
[12]A. M. Goodman, Phys. Rev. **144**, 588 (1966).
[13]J. P. Ganachaud and A. Mokrani, Surf. Sci. **334**, 329 (1995).
[14]Y. J. Chabal, M. K. Weldon, K. T. Queeney, and A. Esteve, in *Fundamental Aspects of Silicon Oxidation*, edited by Y. J. Chabal (Springer, New York, 2001), Vol. 46, Chap. 8, p. 143.
[15]M. K. Gunde, Physica B **292**, 286 (2000).
[16]S. M. Sze, *Physics of Semiconductor Devices* (Wiley, New York, 1969), Chap. 9.
[17]T. Ohmi, M. Morita and T. Hattori, in *The Physics and Chemistry of* SiO_2 *and the Si–*SiO_2 *Interface*, edited by C. Robert Helms (Plenum, New York, 1992), Vol. 2, p. 413.
[18]T. Yoshida, D. Imafuku, J. L. Alay, S. Miyazaki, and M. Hirose, Jpn. J. Appl. Phys., Part 2 **34**, L903 (1995).
[19]J. L. Alay and M. Hirose, J. Appl. Phys. **81**, 1606 (1997).
[20]R. Williams, Phys. Rev. A **140**, A569 (1965).
[21]S. T. Pantelides, A. Selloni, and R. Car, Solid-State Electron. **28**, 17 (1985).
[22]J. Wagner, Phys. Rev. B **29**, 2002 (1984).
[23]S. D. Brorson, D. J. DiMaria, M. V. Fischetti, F. L. Pesavento, P. M. Solomon, and D. W. Dong, J. Appl. Phys. **58**, 1302 (1985).